journal

J. Am. Ceram. Soc., **83** [11] 2737–44 (2000)

Realistic Finite-Element Model for the Double-Torsion Loading Configuration

Matteo Ciccotti

Dipartimento di Fisica, Settore di Geofisica, Università di Bologna, Bologna, Italy

The analytical approach to the double-torsion, constant-displacement-configuration technique has forced a strong oversimplification of the specimen model, and, therefore, of the strain field in classical applications. For the present study, accurate three-dimensional finite-element analysis was performed on a realistic specimen; that is, one with finite thickness, a groove, and an initial notch. The influence on the strain-energy release rate of the specimen width and length, the fracture length, the presence and shape of the side groove, the presence of an initial notch, and the curved shape of the fracture front was estimated from this analysis. Significant deviations from the classical analytical solution were found. The present results should reduce the discrepancies found among measurements made in various laboratories and that traditionally have prevented the development of effectively applicable fracture models.

I. Introduction

THE double-torsion, load-relaxation, constant-displacement-configuration method was developed by Evans[1] to determine the velocity of crack propagation, v, versus the strain-energy release rate, G (G–v curve). A typical double-torsion specimen is shown in Fig. 1(a). According to Williams and Evans,[2] G is given by

$$G = -\left(\frac{dU}{dA}\right)_y = \frac{P^2}{2d_n}\frac{dC}{da} = \frac{w_m^2 P^2}{2\eta W d^3 d_n \mu} \quad (1)$$

where U is the total strain energy, A the crack area, P the measured load, y the constant displacement imposed on the loading points, C the compliance of the specimen, w_m the moment arm of the torsion, W the specimen width, d the specimen thickness, d_n the reduced thickness of the specimen in the region of the groove (see Fig. 1(b)), μ the shear modulus, and η a tabled function of W/d.[4]

Equation (1) is based on the following model. The double-torsion (DT) specimen is a symmetrical system of two independent plates with lengths equal to the crack length, each plate subject to simple torsion. The part of the specimen beyond the fracture tip is considered undeformed. The compression induced by the torsion at the contact zone of the two plates on the upper face is ignored. The presence of the side groove, the effect of its shape, and the presence of the initial notch are ignored. Finally, the model does not account for the fact that the crack has a different extension, Δa, on each of the two faces and a curved profile at its tip (see Fig. 1(c)).

The practical importance of these approximations, made necessary by the analytical approach, is unknown. For this reason, the present study consisted of an accurate, three-dimensional, finite-element analysis of a realistic specimen, that is, one with finite thickness, a groove, and an initial notch. The purpose of the present study was to estimate the influence on G of the specimen width and length, the fracture length, the presence and shape of the side-groove, the presence of the initial notch, and the curved shape of the fracture front.

This approach was explored earlier by Trantina.[5] His results were interesting but not very useful in practice, because his study of 176 linear elements produced only five values of G for a specific specimen with no side groove and no initial notch. Furthermore, his use of linear elements prevented him from obtaining a crack front with a realistic inclination.

II. Finite-Element Model

(1) Choice of the Physical Quantity G

Evans's equation[1] is based on the computation of the strain-energy release rate (SERR) by derivation of the compliance of the DT specimen. He uses the plane-stress relationship to obtain the Mode I stress-intensity factor, K_I. Because the plane-stress assumption and the exact fracture modality are, to date, not well understood in the DT loading configuration, direct measurement of the SERR in the finite-element simulation seems best for studying Evans's equation. The idea is to measure the difference, δU, in

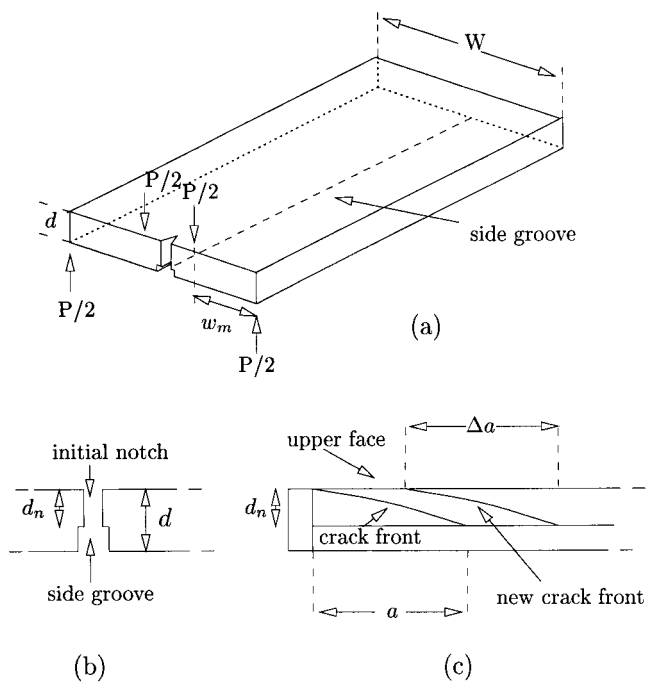

Fig. 1. Sketch of a double-torsion specimen: (a) general view, (b) axial cross section, and (c) longitudinal cross section. (After Atkinson.[3])

A. Jagota—contributing editor

Manuscript No. 189276. Received November 1, 1999; approved May 23, 2000.

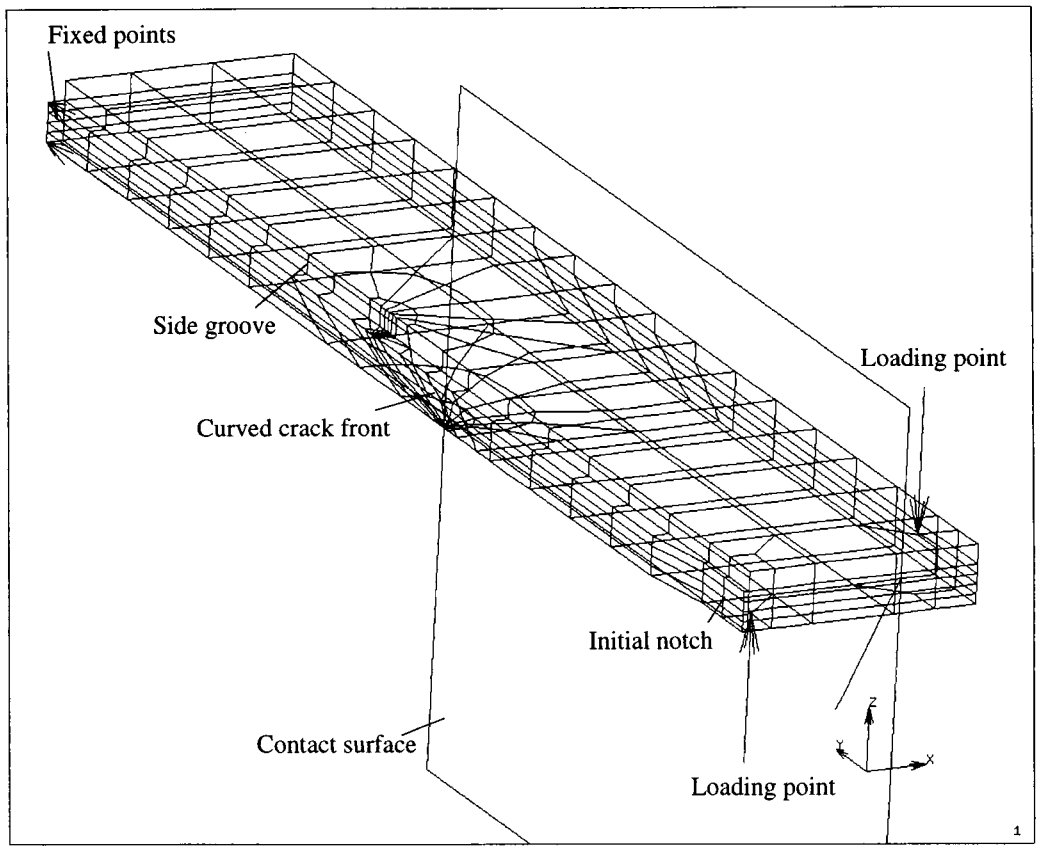

Fig. 2. Finite-element mesh. Model represents one-half of the DT specimen. Remaining part is replaced by symmetrical conditions and by a contact surface along the failed interface. Side groove and initial notch are reproduced. Crack front is designed by hand to represent the experimental shape.

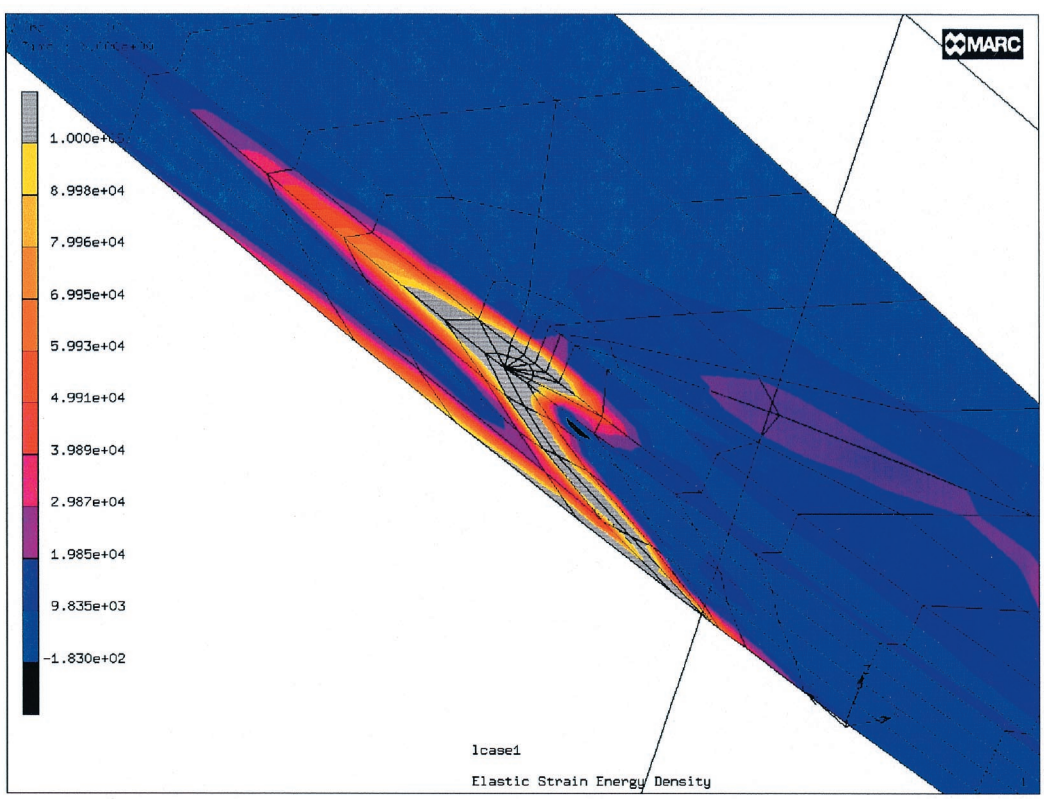

Fig. 3. Plot of the strain-energy density field near the fracture front. Energy is concentrated along the curved front and inside the groove.

Table I. Corrective Factors for Specimens of Length, $L = 17$ cm, and Width, $W = 6$ cm

Grove depth, d_n/d[‡]	Grove width, g_w (mm)	Notch length, nl (cm)	Inclination, c[§]	Corrective factor, ψ				
				$a = 4.5$ cm	$a = 6.5$ cm	$a = 8.5$ cm	$a = 10.5$ cm	$a = 12.5$ cm
1	0	0	0	0.936	0.962	0.966	0.971	1.039
1	0	0	2	0.861	0.950	0.959	0.963	1.038
1	0	0	4	0.774	0.934	0.949	0.956	1.013
2/3	2	0	0	0.944	0.965	0.971	0.987	1.119
2/3	2	0	2	0.938	0.965	0.971	0.987	1.091
2/3	2	0	4	0.925	0.961	0.968	0.981	1.068
2/3	4	0	0	0.968	0.991	0.997	1.021	1.186
2/3	4	0	2	0.962	0.988	0.995	1.015	1.149
2/3	4	0	4	0.948	0.985	0.992	1.010	1.115
1/2	2	0	0	0.964	0.991	0.999	1.048	1.281
1/2	2	0	2	0.961	0.988	1.000	1.040	1.252
1/2	2	0	4	0.952	0.984	0.997	1.034	1.219
1/2	4	0	0	0.977	1.025	1.047	1.118	1.440
1/2	4	0	2	0.973	1.022	1.044	1.111	1.398
1/2	4	0	4	0.964	1.021	1.040	1.099	1.354
1	0	2	0	0.909	0.961	0.965	0.971	1.039
1	0	2	2		0.948	0.961	0.963	1.037
1	0	2	4		0.931	0.948	0.954	1.012
2/3	2	2	0	0.929	0.966	0.969	0.989	1.120
2/3	2	2	2	0.921	0.964	0.972	0.988	1.093
2/3	2	2	4	0.897	0.961	0.968	0.978	1.067
2/3	4	2	0	0.952	0.989	0.996	1.017	1.186
2/3	4	2	2	0.941	0.987	0.994	1.018	1.149
2/3	4	2	4	0.911	0.981	0.992	1.009	1.115
1/2	2	2	0	0.961	0.990	0.998	1.046	1.282
1/2	2	2	2	0.955	0.987	0.998	1.041	1.253
1/2	2	2	4	0.944	0.985	0.995	1.035	1.220
1/2	4	2	0	0.976	1.026	1.045	1.119	1.438
1/2	4	2	2	0.970	1.021	1.044	1.113	1.400
1/2	4	2	4	0.958	1.018	1.040	1.098	1.347

[†]Some data are missing because the curved crack front would cross the initial notch. [‡]Where d_n is the reduced thickness and d the specimen thickness. [§]Of the crack front, expressed as the ratio between the difference, Δa, in the crack length on the two faces and the reduced thickness, d_n.

total strain energy for two meshes with a small difference, δa, in crack length and to normalize δU to the difference in crack area. Thus,

$$G = -\frac{1}{d_n}\left(\frac{\delta U}{\delta a}\right)_y \tag{2}$$

Consequently, the mesh does not have to be very fine, because an extremely accurate representation of the deformation field around the crack tip is necessary only if the crack-surface displacement approach is used.

(2) Finite-Element Code and Computing Resources

The present meshes were designed using a graphic editor (MENTAT 3.2, MARC Corporate, Palo Alto, CA) and analyzed using a parallel code (MARC K7.3, MARC Corporate). The solution process was very laborious, but it was made feasible by access to the powerful resources of the CINECA computing center (Consorzio Interuniversitario Nord-Est Calcolo Automatico, Bologna, Italy) and, in particular, a supercomputer (Model Origin™ 2000, SGI™, Mountain View, CA) with 16 parallel CPUs (MIPS R10 K, 195 MHz), 8 gigabytes of RAM, and a peak performance of 6.24 gigaflops. The operating system used was CELLULAR IRIX 6.5.3 (SGI). Because this supercomputer used ~5 CPU min to solve a model, the present study analyzed 1800 models in 150 CPU h, obtaining 600 values of G that explored combinations of various parameters.

(3) Mesh Design

The finite-element model is designed to represent a DT specimen under a constant-displacement configuration. Because the model is symmetrical, the mesh describes only one-half of the specimen (see Fig. 2). The model consists of ~500 brick elements divided into five slices, one of which is partially removed to simulate the presence of the side groove. Some elements at the beginning of the groove are shrunk to produce an empty space that simulates the initial notch. The refined subdivision of the elements in the first row allows the positioning of the loading points (four-point bending).

The most sophisticated part of the design is the region surrounding the crack. The most common solution for representing cracks is to design a spider-web mesh around the crack front, with quarter-point nodes on the first shell of elements. This solution allows for better adaptation to the physical behavior of the strain field near the crack tip and has been validated against the predictions of the analytical solution for the double cantilever beam.[5]

Trantina[5] also used this spider-web mesh for the DT loading configuration, introducing a weak inclination of the fracture front. Because the strain field near the curved crack tip of the DT specimen was not known in detail, Trantina removed the inner shell of elements near the crack tip. In contrast, the present study involved first testing the elements with quarter-point nodes and then the normal elements; an attempt also was made to remove the inner shell. Because all the variations in G generally were <1%

Table II. Corrective Factors for Specimens of Length, $L = 17$ cm, and Width, $W = 10$ cm

Grove depth, d_n/d[‡]	Grove width, g_w (mm)	Notch length, nl (cm)	Inclination, c[§]	Corrective factor, ψ				
				$a = 4.5$ cm	$a = 6.5$ cm	$a = 8.5$ cm	$a = 10.5$ cm	$a = 12.5$ cm
1	0	0	0	0.892	0.946	0.976	1.038	1.251
1	0	0	2	0.695	0.898	0.932	0.992	1.205
1	0	0	4	0.562	0.859	0.892	0.944	1.113
2/3	2	0	0	0.904	0.958	0.997	1.095	1.430
2/3	2	0	2	0.876	0.938	0.979	1.066	1.361
2/3	2	0	4	0.845	0.917	0.958	1.039	1.297
2/3	4	0	0	0.921	0.975	1.023	1.138	1.529
2/3	4	0	2	0.891	0.954	1.002	1.112	1.457
2/3	4	0	4	0.856	0.931	0.979	1.079	1.384
1/2	2	0	0	0.937	0.999	1.060	1.221	1.721
1/2	2	0	2	0.918	0.984	1.044	1.195	1.646
1/2	2	0	4	0.894	0.969	1.026	1.166	1.586
1/2	4	0	0	0.960	1.037	1.119	1.338	1.987
1/2	4	0	2	0.935	1.020	1.103	1.303	1.902
1/2	4	0	4	0.912	1.004	1.081	1.269	1.804
1	0	2	0	0.835	0.935	0.973	1.038	1.255
1	0	2	2		0.899	0.928	0.986	1.201
1	0	2	4		0.861	0.885	0.940	1.114
2/3	2	2	0	0.856	0.951	0.995	1.096	1.424
2/3	2	2	2	0.836	0.931	0.975	1.067	1.362
2/3	2	2	4	0.799	0.908	0.953	1.037	1.298
2/3	4	2	0	0.874	0.967	1.019	1.140	1.524
2/3	4	2	2	0.847	0.943	1.000	1.110	1.459
2/3	4	2	4	0.805	0.920	0.977	1.078	1.387
1/2	2	2	0	0.908	0.991	1.061	1.221	1.714
1/2	2	2	2	0.883	0.977	1.045	1.190	1.647
1/2	2	2	4	0.856	0.960	1.027	1.167	1.579
1/2	4	2	0	0.924	1.030	1.120	1.339	1.988
1/2	4	2	2	0.897	1.012	1.100	1.304	1.903
1/2	4	2	4	0.865	0.992	1.083	1.270	1.806

[†]Some data are missing because the curved crack front would cross the initial notch. [‡]Where d_n is the reduced thickness and d the specimen thickness. [§]Of the crack front, expressed as the ratio between the difference, Δa, in the crack length on the two faces and the reduced thickness, d_n.

(with better consistency between quarter-point and normal elements), the simpler normal elements were used here. The radius of the inner shell of nodes was $R = 1.6$ mm ($R/d = 0.23$).

The geometry of the inclined spider web was matched carefully with the presence of the groove, and the internal position of each node was optimized, with the purpose of reaching the maximum curved-front inclination allowed by the deformation limits of the elements. (The graphic mesh editor MENTAT has an internal element-check function that highlights elements whose distortion is above a threshold value.)

For the low strain used in the present model, and assuming the use of second-order elements, the code indicated a threshold value of 0.95. In regard to distortion, this value indicated that the internal angles of each element could not decrease below 10°. In regard to the aspect ratio (the ratio between the surface and the volume of an element), the 0.95 threshold value meant that the ratio between the lengths of the different sides of an element could not be >12.

These restrictions limited the extent of curvature of the crack profile. Experimental results have shown that the ratio of inclination, c, between Δa and d_n typically is ~ 5.[1] In the present case, optimization allowed a maximum inclination at $c = 4$, a substantial improvement over the value of $c = 1.7$ obtained by Trantina[5] with lower-order elements. To simulate the curvature, a different inclination was used for each quarter of d_n. For the specimens with $c = 4$, the four inclinations were 30°, 20°, 10°, and 10°. A series of specimens with a straight front ($c = 0$) and a series with an intermediate inclination, $c = 2$ (angles of 49°, 34°, 19°, and 19°) also were designed to clarify the influence of the front inclination. Figure 3 provides a close-up view of the crack tip for $c = 4$, and a plot of the strain-energy density field.

For the specimen represented by the basic mesh, shown in Fig. 2, $L = 17$ cm, $W = 6$ cm, and $d = 7$ mm. The moment arm of the torsion was $w_m = 2$ cm. Longer specimens, with $L = 25$ cm, were generated by adding rows of elements. Wider specimens, with $W = 10$ cm, were generated by expanding the external row of elements, so that only the moment arm was changed, to $w_m = 3.5$ cm, leaving all of the internal region containing the groove unaltered.

For each combination, five crack lengths were obtained by moving the central part with the crack and resubdividing the elements of the remaining parts. The crack-length values, a, were measured from the position of the loading points—in the present case, 0.5 cm from the beginning of the specimen to the end of the crack on the lower opening side. For the shorter specimens, the crack-length (a) values were 4.5, 6.5, 8.5, 10.5, and 12.5 cm; for the longer specimens, the crack-length (a) values were 5.5, 8.5, 12.5, 16.5, and 20.5 cm.

The width of the groove was changed by incrementally decreasing the width of the corresponding row of elements from 4 to 2 mm. The change in depth of the groove, from one-third to one-half of the specimen thickness ($d/3$ to $d/2$), needed more attention: The entire slice under the groove was contracted in the z direction, but the central block surrounding the crack front also had to be contracted by the same amount along the direction of the groove, to preserve the same aspect ratio for the crack-front profile relative

Table III. Corrective Factors for Specimens of Length, $L = 25$ cm, and Width, $W = 6$ cm

Grove depth, d_n/d[‡]	Grove width, g_w (mm)	Notch length, nl (cm)	Inclination, c[§]	Corrective factor, ψ				
				$a = 4.5$ cm	$a = 6.5$ cm	$a = 8.5$ cm	$a = 10.5$ cm	$a = 12.5$ cm
1	0	0	0	0.956	0.966	0.965	0.967	1.046
1	0	0	2	0.922	0.960	0.964	0.965	1.040
1	0	0	4	0.892	0.951	0.956	0.956	1.022
2/3	2	0	0	0.960	0.967	0.968	0.974	1.127
2/3	2	0	2	0.960	0.969	0.966	0.975	1.092
2/3	2	0	4	0.953	0.965	0.967	0.970	1.068
2/3	4	0	0	0.984	0.991	0.992	0.992	1.185
2/3	4	0	2	0.983	0.991	0.992	1.000	1.146
2/3	4	0	4	0.977	0.987	0.992	0.993	1.127
1/2	2	0	0	0.983	0.985	0.991	1.001	1.275
1/2	2	0	2	0.982	0.985	0.989	1.003	1.242
1/2	2	0	4	0.976	0.982	0.986	0.999	1.219
1/2	4	0	0	1.018	1.016	1.022	1.048	1.448
1/2	4	0	2	1.014	1.019	1.022	1.044	1.389
1/2	4	0	4	1.009	1.016	1.018	1.038	1.348
1	0	2	0	0.951	0.965	0.965	0.966	1.041
1	0	2	2		0.960	0.962	0.960	1.043
1	0	2	4		0.946	0.955	0.956	1.020
2/3	2	2	0	0.961	0.967	0.966	0.975	1.128
2/3	2	2	2	0.956	0.968	0.968	0.976	1.093
2/3	2	2	4	0.949	0.967	0.965	0.971	1.069
2/3	4	2	0	0.983	0.991	0.991	1.000	1.187
2/3	4	2	2	0.980	0.990	0.991	0.997	1.148
2/3	4	2	4	0.968	0.987	0.988	0.996	1.121
1/2	2	2	0	0.984	0.990	0.989	1.008	1.276
1/2	2	2	2	0.982	0.986	0.986	1.004	1.242
1/2	2	2	4	0.976	0.983	0.987	0.994	1.220
1/2	4	2	0	1.016	1.023	1.024	1.049	1.439
1/2	4	2	2	1.014	1.016	1.020	1.045	1.390
1/2	4	2	4	1.007	1.014	1.020	1.039	1.349

[†]Some data are missing because the curved crack front would cross the initial notch. [‡]Where d_n is the reduced thickness and d the specimen thickness. [§]Of the crack front, expressed as the ratio between the difference, Δa, in the crack length on the two faces and the reduced thickness, d_n.

to d_n. Specimens without grooves were produced by eliminating the first slice, expanding the remaining part in the z direction, and again expanding the central block along the direction of the groove.

All the present specimens also were doubled in number, to create a version with an initial notch 2 cm long and another without a notch. The parameter values can be summarized as follows.

(1) Five crack lengths of $a = 4.5$, 6.5, 8.5, 10.5, and 12.5 cm for $L = 17$ cm, and five crack lengths $a = 5.5$, 8.5, 12.5, 16.5, and 20.5 cm for $L = 25$ cm.
(2) Three front inclinations of $c = \Delta a/d_n = 0$, 2, and 4.
(3) Three groove depths of $g_d = 1 - d_n = 0$, $d/3$, and $d/2$.
(4) Three groove widths of $g_w = 0$, 2, and 4 mm.
(5) Two specimen lengths of $L = 17$ and 25 cm.
(6) Two specimen widths of $W = 6$ and 10 cm.
(7) Two notch lengths of nl = 0 and 2 cm.

Combining these parameters by Cartesian product resulted in 600 different models (not all combinations are possible). For the computation of G, three meshes were produced for each model, moving forward the region around the crack front in two steps of 0.2 mm each. The two strain-energy increases were verified to be consistent, and the strain-energy release rate on the global increment was calculated.

The total number of meshes analyzed was 1800. To accelerate the design process, only 60 basic meshes were worked out individually with the graphic editor. All the other meshes were generated automatically by moving some sets of nodes using external C programs and Unix shell scripts expressly written for that purpose.

(4) Boundary Conditions

The load was applied using a four-point bending scheme, by imposing a fixed vertical displacement onto the loading points, as shown in Fig. 2. The inner loading point on the bottom face was moved up 0.15 mm, and the outer loading point on the top face was moved down by the same amount, so that the global deformation, y, was 0.3 mm. Because the deformation was not symmetrical with respect to the z direction, all other points had to be free to move vertically for the whole specimen to find its equilibrium position. To prevent other global translations or rotations of the model, two points at the end of the specimen were fixed in the x and y directions (see Fig. 2).

The symmetrical boundary conditions at the interface between the two halves of the specimen were implemented in two steps.

(1) The nodes on the intact portion of the interface were bound to move on a vertical plane.

(2) The nodes of the cracked portion were free to move away from the vertical plane, but they were bound by a rigid contact surface that simulated the compressive effect against the other half of the specimen (see Fig. 2).

The contact surface started before the first node on the top of the cracked surface. In the specimens with a curved crack front, this positioning left out some nodes along the crack surface, but the

Table IV. Corrective Factors for Specimens of Length, $L = 25$ cm, and Width, $W = 10$ cm

Grove depth, d_n/d[‡]	Grove width, g_w (mm)	Notch length, nl (cm)	Inclination, c[§]	Corrective factor, ψ				
				$a = 4.5$ cm	$a = 6.5$ cm	$a = 8.5$ cm	$a = 10.5$ cm	$a = 12.5$ cm
1	0	0	0	0.929	0.962	0.966	0.983	1.251
1	0	0	2	0.841	0.913	0.937	0.946	1.203
1	0	0	4	0.775	0.883	0.898	0.914	1.118
2/3	2	0	0	0.937	0.964	0.972	1.005	1.430
2/3	2	0	2	0.915	0.950	0.958	0.983	1.343
2/3	2	0	4	0.891	0.932	0.939	0.972	1.304
2/3	4	0	0	0.951	0.978	0.982	1.019	1.537
2/3	4	0	2	0.927	0.959	0.966	1.008	1.427
2/3	4	0	4	0.901	0.942	0.953	0.987	1.382
1/2	2	0	0	0.965	0.981	0.987	1.056	1.711
1/2	2	0	2	0.948	0.973	0.985	1.047	1.631
1/2	2	0	4	0.932	0.959	0.970	1.029	1.586
1/2	4	0	0	0.981	1.004	1.014	1.118	1.974
1/2	4	0	2	0.965	0.990	1.002	1.098	1.862
1/2	4	0	4	0.949	0.978	0.987	1.089	1.801
1	0	2	0	0.905	0.959	0.963	0.976	1.254
1	0	2	2		0.908	0.936	0.949	1.205
1	0	2	4		0.876	0.895	0.917	1.109
2/3	2	2	0	0.922	0.963	0.967	0.995	1.431
2/3	2	2	2	0.901	0.946	0.959	0.984	1.344
2/3	2	2	4	0.872	0.927	0.940	0.973	1.305
2/3	4	2	0	0.932	0.974	0.983	1.020	1.522
2/3	4	2	2	0.911	0.959	0.967	1.010	1.444
2/3	4	2	4	0.881	0.940	0.954	0.989	1.383
1/2	2	2	0	0.950	0.985	0.988	1.056	1.712
1/2	2	2	2	0.930	0.974	0.979	1.047	1.631
1/2	2	2	4	0.912	0.960	0.971	1.029	1.587
1/2	4	2	0	0.967	1.001	1.015	1.118	1.975
1/2	4	2	2	0.947	0.987	1.003	1.099	1.883
1/2	4	2	4	0.927	0.972	0.995	1.078	1.802

[†]Some data are missing because the curved crack front would cross the initial notch. [‡]Where d_n is the reduced thickness and d the specimen thickness. [§]Of the crack front, expressed as the ratio between the difference, Δa, in the crack length on the two faces and the reduced thickness, d_n.

omission was not a cause for concern, because loading clearly would move the nodes away from the contact surface.

(5) Element Properties

For the present model, 20-node elements belonging to the serendipity family were used. These second-order elements, characterized by the presence of additional nodes in the middle of each edge, provided a good balance between rapidity of convergence and computational cost. Full integration, based on five points, made the solution more accurate. The analysis was based on linear elasticity, with the physical properties of the material given by the values of Young's modulus, $E = 10^4$ MPa; Poisson's ratio, $\nu = 0.2$; and density, $\rho = 2.2$ kg/dm^3—these values are typical for lava rocks, but the results can be easily scaled to more-suitable values for engineering ceramic materials.

III. Testing Stability

For better control of the solution process, the load application was divided into 10 steps, a method that assured optimal linearity with load. The compliance $C = y/P$ was constant within 10^{-5} up to values of the displacement that were 1 order of magnitude larger than the displacements effectively used.

The convergence control was based on the displacement check. The code calculated the convergence ratio using the equation $CR = \max(\delta u_i)/\max(du_j)$, where CR is the convergence ratio, δu_i the node-displacement increments in the last iteration, and du_j the final displacements. The values of CR were always between 2×10^{-12} and 4×10^{-8}, indicating excellent convergence, because the threshold proposed by the code supporters is 0.05. In this type of analysis, the displacement check is more significant than the residual-force check, which is based on the ratio between the maximum residual force and the maximum reaction force. Because the load is applied only on two nodes, the maximum reaction force is always very high, resulting in very low convergence ratios.

Another important test index is the singularity ratio, SR, which is related to the conditioning number, CN, of the system of linear equations to be solved by the Crout elimination process. CN is defined as the ratio between the highest and the lowest eigenvalues of the system. The SR is an upper boundary for the inverse of the matrix conditioning number ($1/SR \leq CN$).

The number of digits lost in the elimination process is $n_{lost} \approx -\log_{10} SR$. SR values obtained in the present solution were always between 8×10^{-7} and 1.8×10^{-2}; this result indicates a maximum loss of about six digits. Because the code works in double precision—that is, with an internal accuracy of 10^{-12}—the first six digits are not affected by numerical approximations. The numerical precision of the strain energy, U, then, is $<10^{-6}$, but the strain-energy release rate is obtained from differences between two values of U with different crack lengths. The crack-length increment chosen for the present study assured that such differences were never $<0.1\%$ of the strain-energy values. Thus, the numerical precision of the differences was always $<10^{-3}$, a good result, because the global accuracy of the present results was $\sim 1\%$.

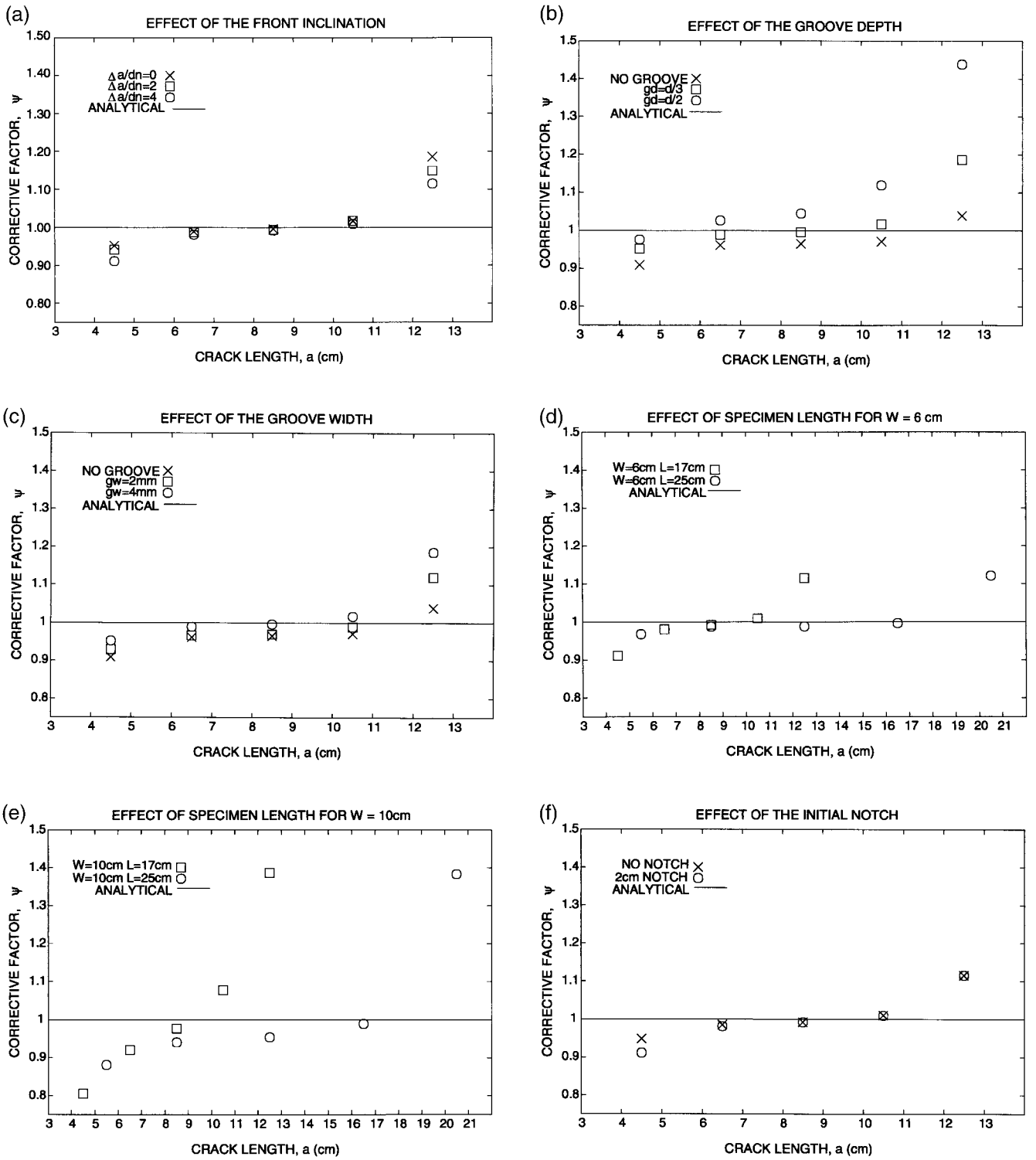

Fig. 4. Effect of the variation of each parameter. For each plot the corrective coefficients, ψ, for the five crack lengths are reported and one parameter is changed: (a) variation of the front inclination, *c*; (b) variation of the groove depth, $g_d = (1 - d_n)$; (c) variation of the groove width, g_w; (d) variation of the specimen length for $W = 6$ cm; (e) variation of the specimen length for $W = 10$ cm; and (f) variations of the notch length, nl.

The full Newton–Raphson iterative procedure was used to solve the meshes. To test the reliability of the procedure for the present case, some solutions were derived using a large-displacement procedure, as well as an updated Lagrange procedure. The obtained results were consistent within 1%. The values for total strain energy were obtained by integrating the strain-energy density over the entire mesh. The high degree of linearity observed suggested the recalculation of the total strain energy using the relationship $U = y(P/2)$, where P is the reaction force at the loading points. The two values were consistent within 10^{-5}, a proof of physical reliability. The consistency between the local trend of strain energy caused by small displacements of the nodes during the calculation of G and the general trend of the strain energy among the five different crack lengths, also was checked.

To test the stability of the model, many different meshes, corresponding to the same geometric model, were designed. The number and position of the rows and the slices were changed, as was the extension of the set of nodes that was moved along with

the crack front. The variations obtained were always <1%, giving the present results a precision of 1%.

IV. Results

The present results, consisting of 600 G values, for all combinations of the various parameters, are reported in Tables I–IV as corrective factors, ψ, with respect to Evans's equation. Thus,

$$G = \psi \frac{w_m^2 P^2}{2\eta W d^3 d_n \mu} \tag{3}$$

More precisely, the finite-element value of G, G_{FE}, was evaluated using Eq. (2), where U is twice the total strain energy obtained by the finite-element analysis of the halved specimen. The load, P, was evaluated using the well-verified equation $U = y(P/2)$, where y is the value of the constant displacement. Finally, the values for G_{FE} were divided by the analytical value, G_{AN}, obtained from Eq. (1) for the same load, P. The values of η for $W = 6$ and $W = 10$ cm were 0.285 and 0.304, respectively.[4]

Some of the present results are plotted in Figs. 4(a)–(f) to show the influence on G of each parameter. The correction value is important. Variations from 10% to 50% are apparent for the five different crack lengths, with a increasing trend, in agreement with other experimental observations.[6,7]

The use of three different front inclinations ($c = \Delta a/d_n = 0$, 2, and 4) produced very consistent results in the center of the specimen (Fig. 4(a)). However, away from the center, the SERR varied by ~8% near the borders, and G increased with inclination. The value of $c = 5$, observed in earlier experiments,[1] was not obtained here, because the distortion of the elements around the crack tip was too high, but such a value could be reasonably expected to produce a slightly higher value of ψ.

Changes in the groove depth produced a general shift in the coefficients, accentuated for long cracks (Fig. 4(b)). The SERR increased by ~5% when the groove depth increased from zero to one-half of the specimen thickness. This major effect resulted from the weakening of the specimen. A similar effect influenced the dependence of G on groove width (G increased by ~4% when the groove width increased from 0 to 4 mm, as shown in Fig. 4(c)).

The dependence of G on specimen dimensions was important and complex. For all the specimen widths considered, short crack lengths exhibited consistent results, but the shorter specimens had an earlier deviation of ψ for large values of a (Figs. 4(d) and (e)). This deviation showed that the increase in ψ for long cracks was some type of an end effect. Furthermore, a comparison of Figs. 4(d) and (e) showed a higher deviation for the larger specimen. These results were in agreement with earlier experimental observations[6,7] and also with Fuller's[8] conclusion that such effects should be evaluated in terms of distance of the fracture from the ends of the specimen (expressed in units of width) rather than in terms of the ratio between crack and specimen length.

The difference caused in the SERR by the presence of the initial notch was generally very weak, except for short crack lengths, in which it produced variations of ~5% (Fig. 4(f)).

V. Conclusions

The present finite-element analysis showed that the classical equation for describing DT fracture experiments generally was inadequate. The presence and shape of the side groove, along with the presence of the initial notch, the crack-front shape, and the end effects, were important in affecting the strain-energy release rate. The effect on G of all these parameters was examined exhaustively in the present study in terms of corrective coefficients of the classical equation. The importance of the corrections proved to be considerable (up to 40%) and likely a major cause of the large scatter among the G–v curves measured in various laboratories. Further developments may be found in a companion paper.[9]

Acknowledgments

I thank F. Mulargia for the helpful criticism about the double-torsion model; G. Gonzato for the help in the workout of the scripts for automatic mesh generation; F. Mariani from Espri-MARC (Genova, Italy) for the careful examination of the good fitness of my finite-element models; and the CINECA computing center in Bologna, which provided powerful computing resources and technical support.

References

[1]A. G. Evans, "A Method for Evaluating the Time-Dependent Failure Characteristics of Brittle Materials—And Its Applications to Polycrystalline Alumina," *J. Mater. Sci.*, **7** [10] 1137–46 (1972).

[2]D. P. Williams and A. G. Evans, "A Simple Method for Studying Slow Crack Growth," *J. Test. Eval.*, **1** [4] 264–70 (1973).

[3]B. K. Atkinson, "Technical Note," *Int. J. Rock Mech. Miner. Sci. Geomech. Abstr.*, **16**, 49–53 (1979).

[4]S. Timoshenko and J. N. Goodier, *Theory of Elasticity*, 2d ed.; p. 277. McGraw-Hill, New York, 1951.

[5]G. G. Trantina, "Stress Analysis of the Double-Torsion Specimen," *J. Am. Ceram. Soc.*, **60** [7–8] 338–41 (1977).

[6]B. J. Pletka, E. R. Fuller Jr., and B. G. Koepke, "An Evaluation of Double-Torsion Testing—Experimental"; pp. 19–37 in *Fracture Mechanics Applied to Brittle Materials*, ASTM STP 678. American Society for Testing and Materials, Philadelphia, PA, 1979.

[7]D. K. Shetty and A. V. Virkar, "Determination of the Useful Range of Crack Length in Double-Torsion Specimens," *J. Am. Ceram. Soc.*, **61** [1–2] 93–94 (1978).

[8]E. R. Fuller Jr., "An Evaluation of Double-Torsion Testing—Analysis"; see Ref. 6, pp. 3–18.

[9]M. Ciccotti, G. Gonzato, and F. Mulargia, "The Double-Torsion Loading Configuration for Fracture Propagation: Improvement of the Methodology for the Load-Relaxation at Constant Displacement," *Int. J. Rock Mech. Min. Sci.*, in press. □